ARL-TR-8936 ● Apr 2020

Aerodynamic Design Optimization of Long-Range Projectiles Using Missile DATCOM

by Joseph D Vasile, Joshua T Bryson, and Frank E Fresconi

NOTICES

Disclaimers

ARL-TR-8936 ● APR 2020

Aerodynamic Design Optimization of Long-Range Projectiles Using Missile DATCOM

Joseph D Vasile, Joshua T Bryson, and Frank E Fresconi
Weapons and Materials Research Directorate, CCDC Army Research Laboratory

REPORT DOCUMENTATION PAGE			*Form Approved* *OMB No. 0704-0188*

1. REPORT DATE *(DD-MM-YYYY)* April 2020	**2. REPORT TYPE** Technical Report	**3. DATES COVERED (From - To)** 1 June 2018–1 August 2019
4. TITLE AND SUBTITLE Aerodynamic Design Optimization of Long-Range Projectiles Using Missile DATCOM		**5a. CONTRACT NUMBER**
		5b. GRANT NUMBER
		5c. PROGRAM ELEMENT NUMBER
6. AUTHOR(S) Joseph D Vasile, Joshua T Bryson, and Frank E Fresconi		**5d. PROJECT NUMBER**
		5e. TASK NUMBER
		5f. WORK UNIT NUMBER
7. PERFORMING ORGANIZATION NAME(S) AND ADDRESS(ES) CCDC Army Research Laboratory ATTN: FCDD-RLW-LE Aberdeen Proving Ground, MD 21005		**8. PERFORMING ORGANIZATION REPORT NUMBER** ARL-TR-8936
9. SPONSORING/MONITORING AGENCY NAME(S) AND ADDRESS(ES)		**10. SPONSOR/MONITOR'S ACRONYM(S)**
		11. SPONSOR/MONITOR'S REPORT NUMBER(S)

12. DISTRIBUTION/AVAILABILITY STATEMENT

Approved for public release; distribution is unlimited.

13. SUPPLEMENTARY NOTES

ORCID ID(s): Joseph D Vasile, 0000-0003-3812-6277; Joshua T Bryson, 0000-0002-0753-6823

14. ABSTRACT

The goal of this study was to utilize a quick and robust semi-empirical aerodynamics prediction code (Missile DATCOM) to optimize and improve understanding of the flight performance for long-range guided projectiles. Multiple optimal designs were found based on flow regime (i.e., subsonic or supersonic), projectile geometry (i.e., diameter, length-to-diameter, and ogive length), and control configuration (e.g., Body-Fin). A weighted multi-objective Particle Swarm Optimization algorithm was implemented to find the control surface sizing that maximized the lift-to-drag, minimized drag, and met a static margin value for the vehicle at a given body angle of attack. An inviscid computational fluid dynamics solver (i.e., Cart3D) was applied to the optimal configurations and combined with the semi-empirical predictions in a formal manner to improve the accuracy of the aerodynamic model and coefficients. These aerodynamics underpin both 3 and 6 degree-of-freedom simulations to evaluate flight performance. The results from the higher fidelity aerodynamic simulations showed good agreement with the semi-empirical aerodynamic predictions. Outputs of the optimization routine along with the comprehensive flight characterization indicated that the optimization approach is an efficient tool for producing favorable long-range gliding projectiles.

15. SUBJECT TERMS

Particle Swarm Optimization, aerodynamic design optimization, lift-to-drag, long-range guided projectiles, Missile DATCOM

16. SECURITY CLASSIFICATION OF:			**17. LIMITATION OF ABSTRACT**	**18. NUMBER OF PAGES**	**19a. NAME OF RESPONSIBLE PERSON** Joseph D Vasile
a. REPORT Unclassified	**b. ABSTRACT** Unclassified	**c. THIS PAGE** Unclassified	UU	27	**19b. TELEPHONE NUMBER (Include area code)** (410) 306-1794

Standard Form 298 (Rev. 8/98)
Prescribed by ANSI Std. Z39.18

Contents

List of Figures

List of Tables

Acknowledgments

The authors would like to thank Mr Joshua Doyle and Mr Christopher Rosema, US Army Combat Capabilities Development Command (CCDC) Aviation and Missile Center , for their help and discussions regarding Missile DATCOM fundamentals and techniques. This work was supported in part by a grant of high-performance computing time from the US Department of Defense (DOD) High Performance Computing Modernization program at the CCDC Army Research Laboratory DOD Supercomputing Resource Center (DSRC), Aberdeen Proving Ground, Maryland, and the US Army Engineer Research and Development Center, Vicksburg, Mississippi.

1. Introduction

Recently, there has been great emphasis on investigating technologies and methodologies that can extend the weapon range of guided munitions in order to provide better coverage of the battlefield. The primary focus of the current work is to develop an efficient design tool that provides flight vehicle designs that exhibit favorable aerodynamic performance (i.e., high lift-to-drag) in order to reach significant ranges. The typical design method of guided munitions is an iterative process that begins with a baseline concept that undergoes continual modifications until performance requirements are met. The aerodynamic portion of the design process requires a considerable amount of evaluations (e.g., wind tunnel experiments, computational fluid dynamics [CFD], flight trajectory simulation), and ultimately may not result in the optimal configuration. More recently, aerodynamic design optimization methods have become more integrated into the design process, resulting in better final designs while drastically reducing time and costs. Several studies have used optimization to determine the exterior shape (e.g., nose) as well as sizing of control surfaces (e.g., canard and tail fin planform area) of both guided and unguided missiles to maximize flight performance.[1–6]

A weighted multi-objective Particle Swarm Optimization (PSO) algorithm was implemented to find the control surface sizing of a projectile at a given body angle of attack. PSO is a stochastic, population-based computer algorithm that applies the concept of swarm intelligence to problem solving.[7–8] Swarm intelligence is the property of a system whereby the collective behaviors of particles interacting locally with their environment cause coherent functional global patterns to emerge. A physical analogy might be a swarm of bees searching for a food source; each bee makes use of its own memory as well as knowledge gained by the swarm as a whole to find the best available food source.[9] Compared to other optimization techniques, PSO is a simple algorithm that can be implemented fairly easily. PSO is a metaheuristic, gradient-free optimization method that is very useful for many practical engineering design applications where gradient-based methods encounter difficulties (e.g., non-differential functions, disconnected or discrete feasible space, multiple local extrema). Although PSO is a population-based algorithm, it works well with relatively few particles (e.g., 10 to 40) and there are no “generations” or selection operations; design variables are directly updated each iteration. Several studies have been explored to improve the performance of PSO, including adjusting parameters of the search behavior, or modifying the algorithm to ultimately improve convergence efficiency.[10–12]

Most studies that apply optimization methods to determine aerodynamic shapes incorporate a computationally inexpensive tool to evaluate designs; this is due to the inherent nature of any optimization algorithm. The evaluation of each new design is necessary to determine if the current design is suitable for the given objective. Therefore, in order to maintain efficiency and time savings, either semi-empirical aerodynamic prediction (SEAP) codes[5] or Euler CFD solvers[13–14] are incorporated with optimization methods to determine optimal aerodynamic designs.

In the current work, an automated design optimization routine was developed and implemented to recommend aerodynamic characteristics (i.e., size of the control surfaces) to maximize the lift-to-drag ratio (*L/D*) for each projectile for a given diameter, length-to-diameter ratio, and ogive length. Specifically, the PSO method incorporated with the SEAP code Missile DATCOM[15] to determine the optimal design for each configuration. Additionally, NASA's Cartesian Euler CFD analysis package Cart3D[16] was used to further analyze each optimal design. A formal process to combine these multiple sources into an aerodynamic dataset is outlined. This aerodynamic model and these coefficients underpin both 3-degree-of-freedom (DOF) and 6-DOF modeling. Flight trajectory simulations are necessary to evaluate flight system performance.

2. Vehicle Configurations

The focus of the research was to determine the optimal control surface design for a given vehicle configuration. Multiple vehicle configurations incorporating different control configurations (i.e., canards, wings, and fins) were investigated; however, only the Body-Fin configuration will be addressed in this report. Recent results from flight trajectory simulation indicate that tail-fin control flight vehicles perform better in extending range than compared to canard-control configurations. More details regarding the optimization process for both Body-Fin-Canard and Body-Fin-Canard-Wing vehicle configurations are discussed in Strohm et. al.[17] For each vehicle configuration, the control surface size, shape, and location was found for a given axisymmetric baseline body shape based on diameter, length-to-diameter, and ogive length, as well as for Mach regime of interest (i.e., subsonic or supersonic).

2.1 Baseline Body Projectiles

The general size of the baseline body projectile is determined based on values of diameter of the center body portion of the projectile (i.e., 3, 4, 5, and 6 inches), length-to-diameter ratio (i.e., 6, 8, 10, and 12) and ogive length (i.e., 0.3 and 0.5 of

OAL). A total of 32 body configurations were optimized for each vehicle configuration. The overall length of the flight vehicle (OAL) is determined based on the given diameter and length-to-diameter parameters. The nose tip was modeled as a blunt nose defined by a bluntness radius that is 0.1 of the diameter (i.e., 0.1 caliber). The Von-Karman ogive nose shape was used, with the length of the ogive section defined by the percentage of overall length of the projectile. The center of gravity location of the flight vehicle was defined to be 0.6 of the OAL from the nose for all configurations. This center of gravity value estimate was based on preliminary airframe solid modeling in conjunction with subject matter expertise. The body section was modeled as a constant axisymmetric cylinder. Additionally, a 7° boattail was modeled beginning 0.5 caliber forward of the base. The parameters that were used to determine each baseline body projectile are listed in Table 1.

Table 1 Parameters for baseline body projectiles

Diameter (inch)	Length-to-diameter	Ogive length of OAL	Nose bluntness radius (cal)	Nose ogive shape	Boattail length (cal)
[3, 4, 5, 6]	[6, 8, 10, 12]	[0.3, 0.5]	0.1	Von-Karman	0.5

2.2 Body-Fin Configurations

The optimization routine was implemented to determine the sizing of the control surfaces for each baseline body projectile. For the Body-Fin configuration, the fin set geometry was optimized. A specific set of constraints were placed on the number and overall dimensions of the fins for each vehicle configuration. The Body-Fin configuration was constrained to a total number of 4, 6, or 8 fins. All control surfaces were modeled as simple hex fin cross sections, where a leading and trailing edge wedge were defined as 0.25 of the chord length each with a flat section defined as 0.5 of the chord length at both root and tip of the fin. A total thickness of 4 mm during the flat section for all control surfaces was used.

The number of design variables are specific to each vehicle configuration and are constrained based on speed regime of interest. For the Body-Fin configuration at the subsonic flow regime, in which the objective function was optimized across subsonic Mach (i.e., $M_\infty = 0.5$ to 0.9), the fin root chord was able to vary from 1–3 cal, and the tip-to-tip span of the fin was able to vary from 1.1 to 2 cal or a maximum length of 0.2032 m (i.e., 8 inches). Whereas, for the supersonic flow regime (i.e., objective function optimized across $M_\infty = 1.2$–4), a fin sizing rule where the tip-to-tip span was constrained to 8 inches (i.e., 0.2032 m) but the fin chord was able to vary from 3 to 8 calibers was implemented. For all subsonic flow regime cases, the leading edge sweep angle of the fins was set to 60°, whereas for the supersonic flow cases a leading edge sweep angle of 83° was used. A schematic of the optimal Body-Fin configurations for a given baseline body projectile for both speed regimes of interest is presented in Fig. 1. The parameters that were used to determine the fin set for each configuration are listed in Table 2.

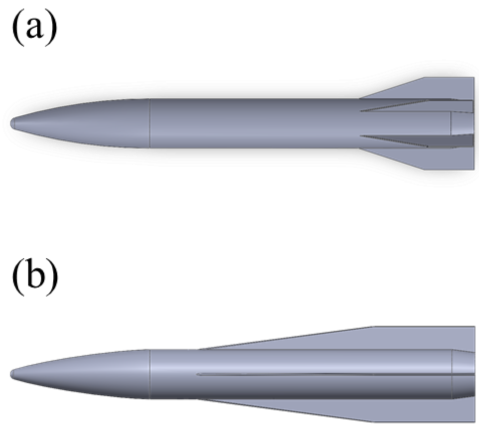

Fig. 1 Optimal Body-Fin configuration for a 4-inch diameter, length-to-diameter of 10, and ogive length of 30% of overall length projectile, for a) subsonic and b) supersonic speeds

Table 2 Fin set design parameters for Body-Fin vehicle configuration

Vehicle configuration	No. of fins	Fin chord (cal)	Fin span (cal)	Fin LE angle
Body-Fin	[4, 6, 8]	[1-3] (M_∞=0.5–0.9), [3-8] (M_∞=1.2–4)	[1.1–2 or 0.2032 m]	[70°] (M_∞ =0.5–0.9), [83°] (M_∞=1.2–4)

2.3 Optimization Tools

2.3.1 Particle Swarm Optimization (PSO)

The essence of the PSO algorithm is that each particle in a swarm represents a design point that can move in the given design space (defined by the number of design variables) looking for the best solution. Each particle's position is updated based on the memory of each particle as well as the knowledge gained by the swarm as a whole. The basic formulation of the algorithm is updating a particle's position and velocity at each iteration until convergence is achieved. The scheme for updating the position of each particle is shown in Eq. 1.

$$x_{k+1}^i = x_k^i + v_{k+1}^i \Delta t \quad (1)$$

where x_{k+1}^i and x_k^i represents the position of particle i at iteration k + 1 and k, respectively, and v_{k+1}^i represents the corresponding velocity of the particle. The velocity of the particle is defined in Eq. 2.

$$v_{k+1}^i \Delta t = w_k^i v_k^i \Delta t + c_1 r_1 \left(p_k^i - x_k^i\right) + c_2 r_2 \left(p_k^g - x_k^i\right) \qquad (2)$$

where r_1 and r_2 are random numbers between 0 and 1, p_k^i is the best position found by particle i so far, p_k^g is the swarm's best particle position at iteration k, v_k^i is the current motion of the particle, w_k^i is the inertia of the particle, c_1 is the cognitive parameter (confidence in itself), and c_2 is the social parameter (confidence in the swarm). The inertia weight of the particle, w_k^i, controls the exploration properties of the algorithm (i.e., larger values enable more global search behavior, whereas smaller values result in more local search behavior). The original PSO algorithm sets constant values for w_k^i, c_1, and c_2; however, further research has demonstrated improved performance when the inertia parameter was set to be adaptive—inertia values would decrease as the algorithm got closer to the optimal solution in order to avoid overshoot. Furthermore, setting the confidence parameters, c_1 and c_2, equal to each other was also found to improve performance. In the current work, c_1 and c_2 were both set to 1, and the inertia parameter was set to be adaptive. The adaptive inertia weight factor developed by Qin et. al.[12] was implemented and is shown in Eq. 3.

$$w_k^i = 1 - \alpha_{PSO} \left(\frac{1}{1+e^{-ISA_k^i}}\right) \qquad (3)$$

where α_{PSO} is a positive constant between 0 and 1 and is set to 0.3 in the current study, and ISA is defined as the Individual Search Ability[12] for each particle and is expressed in Eq. 4.

$$ISA_k^i = \frac{\left|x_k^i - p_k^i\right|}{\left|p_k^i - p_k^g\right| + \epsilon} \qquad (4)$$

where ϵ is a positive constant close to zero, (i.e., $\epsilon = 1 \times 10^{-6}$). The ISA allows for the particle to dynamically adjust to either increase or decrease the inertia weight depending on the relationship between x_k^i, p_k^i, and p_k^g at each iteration. If x_k^i and p_k^i are close and far from p_k^g, ISA decreases, inertia weight increases, and global exploration behavior is enhanced to avoid convergence to a local optimal, whereas if x_k^i is far from p_k^g and p_k^i is close to p_k^g, ISA increases and inertia weight decreases to reduce the global exploration behavior.

Figure 2 illustrates the PSO velocity and position update scheme for each particle. Table 3 summarizes the PSO algorithm.

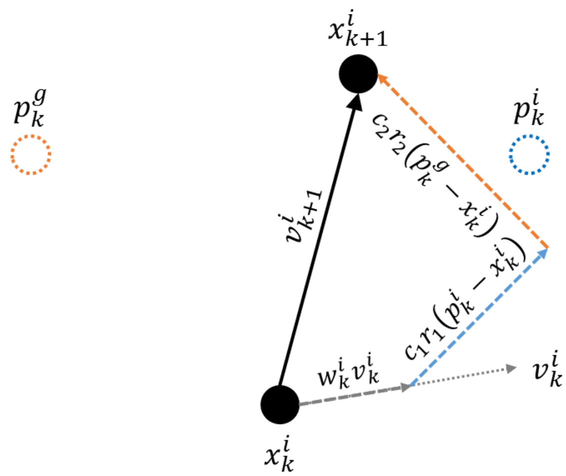

Fig. 2 PSO particle velocity and position update scheme

Table 3 PSO algorithm

1. Initialize a set of particle positions, x_0^i, randomly distributed throughout the design space, and randomly assign velocities, v_0^i, to each particle, or assign zero initial velocities
2. Evaluate each particle's position using the objective function, $f(x_k^i)$
3. Update the best particle position, p_k^i, so far for each particle, the best particle position in the current swarm, p_k^g, and the adaptive inertia weight factor, w_k^i
4. Calculate the updated velocity vector for each particle in the swarm, v_{k+1}^i
5. Update the position of each particle using its previous position and updated velocity, x_{k+1}^i
6. Repeat steps 2–5 until a desired convergence criterion is met

The initial swarm is generated by randomly distributing the set of particles throughout the design space. The position of each initial particle is presented in Eq. 5.

$$x_0^i = x_{min} + r_1(x_{max} - x_{min}) \tag{5}$$

where r_1 is a random number between 0 and 1, and x_{min} and x_{max} are the lower bounds and upper bounds of each given design variable, respectively. The initial velocity for each particle, v_0^i, was set to zero. These positions are then evaluated through the objective function to determine which particle has the best global value in the current swarm, p_k^g, as well as to track each particle's best position so far, p_k^i. The velocity of each particle is then updated using the relationship shown in Eq. 2, which in turn results in a new position for the next iteration (see Eq. 1). These new particle positions are then reevaluated through the objective function (defined later), and a new set of velocities and corresponding positions are computed for each particle. This process of velocity update, position update, and evaluation repeats until a convergence criterion is met. The convergence criterion for the implemented PSO algorithm is based on the variance of the swarm's fitness presented by Tian.[18] The convergence criterion is met when the variance of the function values are below a certain tolerance (i.e., $\epsilon_{tol} = 1 \times 10^{-5}$). The convergence criterion used is presented in Eq. 6.

$$\frac{\sum_{i=1}^{n}\left(\frac{f_i-\bar{f}}{max([1\ max(|f_i-\bar{f}|)])}\right)^2}{n} < \epsilon_{tol} \tag{6}$$

where f_i is the fitness of the i^{th} particle, (i.e., $f(p_k^i)$), $\bar{f}$ is the current mean fitness of the swarm (i.e., $\frac{\sum_{i=1}^{n} f(p_k^i)}{n}$), and n is the number of particles in the swarm. In the current study, a total of 100 particles were used in the swarm. The optimization routine terminates when the particles in the swarm converge to the same point in the design space, in which the variance of the population's fitness is close to zero.

2.3.2 Missile DATCOM

The analysis and ranking of each configuration needed to be completed fairly quickly since PSO utilizes many particles (or design points) in the swarm population per iteration, and carries the swarm population forward in time for many iterations. As the static aerodynamic forces and moments from multiple angles of attack needed to be computed in order to assess each configuration's fitness based on the given objective function at each iteration, a SEAP code was desirable since all aerodynamic coefficients for a given configuration could be computed in a matter of seconds. The SEAP code Missile DATCOM (release 2014)[15] was used to predict the aerodynamic forces and moments for all configurations at 12 Mach numbers (i.e., M_∞ = 0.1, 0.2, 0.4, 0.6, 0.8, 0.9, 1.02, 1.2, 1.5, 2, 3, 4) and at seven angles of attack (α = 0°, 2°, 4°, 6°, 8°, 10°, and 12°).

Missile DATCOM is an engineering-level computer program for estimating aerodynamic stability and control characteristics of conventional missile configurations. It utilizes both theoretical and empirical methods to encompass the entire speed regime from subsonic to hypersonic flight. In previous versions of Missile DATCOM, predictions of vortex-fin interactions (i.e., shedding vortices from upstream control surfaces impacting downstream tail fins) were poor due to insufficient modeling capabilities. However, more recently, the US Army Combat Capabilities Development Command Aviation and Missile Center (CCDC-AvMC) has made significant improvements to the vortex modeling capabilities, including improved fin-shed and body-shed vortex models.[19–20] These improvements allow for better predictions of complex flow interactions, such as vortex-induced flow phenomena (e.g., induced roll for canard-controlled projectiles).

2.3.3 Optimization Architecture

The entire optimization routine was written in and executed using MATLAB[21] on a standalone laptop. MATLAB's object-oriented program definition was used to efficiently create the input files for each desired design configuration. Additionally, the parallel processing computing toolbox was utilized to execute Missile DATCOM in parallel (i.e., four workers) in order to quickly compute the swarm particles for a given iteration. The PSO algorithm automatically steered the optimization process, including initializing the swarm, evaluating the fitness for each design configuration, preparing and executing the Missile DATCOM runs, and updating the next swarm of design configurations. The static aerodynamic coefficients from each Mach number and angle of attack for each design configuration were then collated, and evaluated through the objective function. After the fitness of each configuration was evaluated, a new swarm of design configurations were selected. The process repeated until the convergence criterion was met. The optimization routine was repeated for each of the 32 body baseline projectiles presented in Table 1, for each vehicle configuration (e.g., Body-Fin).

2.3.4 Optimization Problem Definition

The PSO algorithm was implemented to solve a weighted multi-objective optimization problem for each studied baseline body projectile (i.e., diameter [d], length-to-diameter [l/d], and ogive length [l_o]) for a given vehicle configuration (e.g., Body-Fin, Body-Fin-Canard). The optimal configuration is the design that maximizes the weighted objective function: maximizes lift-to-drag ratio, minimizes drag, and minimizes the residual between the static margin (i.e., distance between center of gravity and center of pressure locations) of the vehicle to a desired value at a given body angle at either subsonic (M_∞ = 0.1–0.9) or supersonic (M_∞ = 1.2–4) speeds. Each vehicle configuration has a specific set of design variables (e.g., chord and span of control surface) that can be optimized for each baseline body projectile studied. The PSO algorithm together with Missile DATCOM was used to determine the optimal configurations.

2.3.5 Objective Function

The goal of the optimization process is to determine the flight vehicle design that maximizes the objective function. A weighted sum objective function that combines the lift-to-drag ratio, drag, and static margin value (i.e., $-C_m/C_N$) for given vehicle design at a body angle of attack of 8° was studied and is presented in Eq. 7.

$$f(x) = \sum_i w_1 \left(\frac{L}{D}\right)_i + w_2 \left(\frac{1}{D}\right)_i + w_3 \left(f\left(\frac{-C_m}{C_N}\right)\right)_i \tag{7}$$

where the w_1 is the weight for the lift-to-drag values, which was set to be 2/7; w_2 is the weight for the drag terms, where the inverse drag value was maximized, which was set to be 1/7; and w_3 is weight associated to the piecewise exponential function, $f\left(\frac{-C_m}{C_N}\right)$, which was set to be 4/7.

For both lift-to-drag ratio and drag, the sum of each respective value was summed across Mach number studied. The static margin value at these flight conditions was then evaluated through a piecewise natural exponential function, defined as $f\left(\frac{-C_m}{C_N}\right)$ (i.e., combination of e^x and e^{-x}), which produced a maximum value of 1 when the exponent of the function (i.e., the difference of the exhibited static margin value of the configuration from a desired static margin value) equaled 0 at each given Mach number. The desired static margin value was set to be either 1 (subsonic regime) or 0.3 (supersonic regime) calibers for each Mach number of interest at a body angle of attack 8°. The 8° body angle was selected to match the predicted trim angle for the vehicle; it is expected that the Body-Fin configurations would trim at approximately 8° with trailing edge flap deflection. The constraints of the objective function were constructed such that the design configuration can be evaluated for static stability. If a configuration was unable to meet the constraints, the objective function returned a large negative value such that the optimization routine would naturally deviate from the given design point.

2.4 Aerodynamic Characterization Using Higher Fidelity Simulations: Cart3D

After an optimal design was found, higher fidelity simulations were performed to evaluate the accuracy of the optimizer as well as the performance of the optimal design. NASA's Cartesian Euler CFD analysis package Cart3D (1.5.5)[16] was used to perform aerodynamic analyses for a subset of the found optimal geometries. For each given optimal design, static aerodynamic coefficients from multiple angles of attack were computed. The Euler code was desirable since static aerodynamic coefficients for a given angle of attack could be computed in a matter of minutes.

Cart3D quickly creates a Cartesian computational grid around the geometry after setting the domain's extent and resolution. The process is able to automatically increase fidelity of the domain near small features and curvature of the geometry, therefore better resolving the flow features present near the surface. The domain extended approximately 14 projectile lengths in all directions from the center of the projectile, and the smallest typical grid size for the domain was approximately 1 × 1 × 1 mm (Fig. 3). Mesh density regions were defined to refine the mesh near the surface as well as in the wake region in order to help resolve flow structures. The typical computational domain consisted of approximately 10 million Cartesian cells. Once the mesh is generated, the flow solver (flowCart) exploits the features of the Cartesian grid to quickly compute aerodynamic forces and moments experienced by the configuration. Since the Euler equations being solved do not include the viscous components, the Cart3D analysis package provides only inviscid aerodynamic coefficients. The drag force computed by the inviscid solver is the least accurate since the drag computed neglects the contribution due to skin friction.

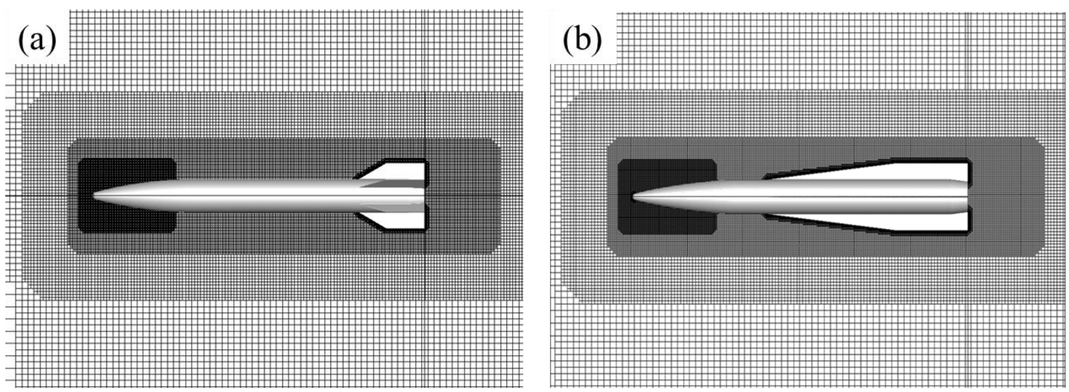

Fig. 3 Computational domains for given optimal designs used for Cart3D: a) subsonic and b) supersonic

3. Results and Discussion

3.1 Aerodynamic Design Optimization

The optimizer typically converged to a design approximately within 50 iterations when using 100 swarm particles for a given vehicle configuration. The optimal design for the Body-Fin configuration for a given baseline body projectile of 4-inch diameter, length-to-diameter of 10, and ogive length of 30% of the overall length of the projectile for both subsonic and supersonic speeds were found and presented in Fig. 3a and b, respectively.

The results of the optimization routine for the given Body-Fin Configurations (i.e., $d = 4$ inches, $l/d = 10$, $l_o = 0.3$) are summarized in Table 4. The optimization routine was able to find the design that maximized the weighted objective function at an assumed body trim angle of 8° for the given Mach regime of interest. The optimizer trended towards the maximum span constraint for all designs in order to maximize the lift of the vehicle. For the given body configuration, both subsonic and supersonic designs converged to the maximum 8-inch fin span. The fin chord for the supersonic configuration was then sized based on the calculated center of pressure location of the vehicle, such that the static margin value of 0.3 was met. Since the subsonic configuration fin set was constrained to meet a desired static margin of 1, additional fins were necessary to improve static stability.

Table 4 Summary of optimization routine for a given vehicle configuration

Vehicle configuration	Diameter (inch)	Length-to-diameter	Ogive length of OAL	No. of fins	Fin chord (cal)	Fin span (cal)
Body-Fin (M_∞=0.5–0.9)	4	10	0.3	6	2	2
Body-Fin (M_∞=1.2–4)	4	10	0.3	4	6	2

The lift-to-drag ratios across angle of attack and Mach number for both optimal subsonic and supersonic designs for the given Body-Fin configurations computed from Missile DATCOM are presented in Fig. 4a and b, respectively.

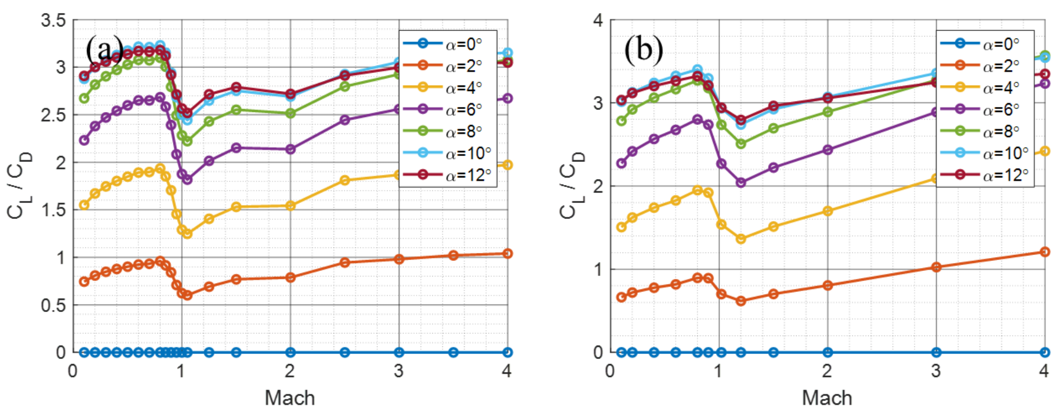

Fig. 4 Lift-to-drag ratios of both optimal a) subsonic and b) supersonic designs for Body-Fin configuration of 4-inch diameter, length-to-diameter of 10, and an ogive length of 30% of the overall length

The computed lift-to-drag ratios show that the optimal vehicle designs achieve values of approximately 3 at body angle of attack of 8° for each respective Mach regime of interest. Both configurations show that the maximum values of lift-to-drag the vehicles could achieve is approximately 3.1. The results indicate that the desired body trim angle for these vehicles is approximately 10°. Furthermore, the results show that lift-to-drag ratios reduce considerably at transonic and low supersonic speeds, indicating that drag substantially increases. The wave drag produced in this regime is a large contributor to the overall detriment in performance. Although the results from Missile DATCOM indicate that the lift-to-drag ratios continue to climb at higher Mach, future Navier-Stokes CFD analysis will need to be performed to explore the hypersonic performance and add confidence to these preliminary results.

3.2 Aerodynamic Characterization of Optimal Design

Higher fidelity simulations were performed to validate the design found from the optimization process. The inviscid flow solver package Cart3D was used to compute the static aerodynamic coefficients across angle of attack and Mach numbers and were compared to the results found from Missile DATCOM. Figure 5 presents the axial force (a-b), normal force (c-d) and pitching moment (e-f) coefficients across angle of attack and Mach for both subsonic (a, c, e) and supersonic (b, d, f) optimal Body-Fin configurations computed from both Missile DATCOM and Cart3D.

Overall, the results from both Missile DATCOM and Cart3D show good agreement. The axial force computed by the Cart3D is expected to be low since the inviscid flow assumption neglects viscous effects, specifically, the skin friction component of drag. The normal force coefficients computed from both methods compare well at small angles of attack across Mach number. At higher angles of attack, the values deviate, suggesting that high angle of attack nonlinear flow physics are present and are not well predicted in the semi-empirical prediction code. However, for body angles of attack less than 8°, Missile DATCOM is able to predict normal force relatively accurately for both finned projectiles across Mach. The largest discrepancies are observed for the predicted pitching moment coefficients. The main contributor to this effect is the difference in the predicted location of the center of pressure between Missile DATCOM and Cart3D. These differences are more exaggerated for the optimal supersonic configuration. Although the normal force was accurately predicted, the center of pressure location, and therefore pitching moment, was not predicted well. Overall, the Cart3D results show larger values of pitching moment, specifically at lower angles of attack. The results suggest that Missile DATCOM may provide a more conservative (i.e., center of pressure location predicted further forward, therefore reduced stability) result when determining the static stability of low aspect ratio fin configurations.

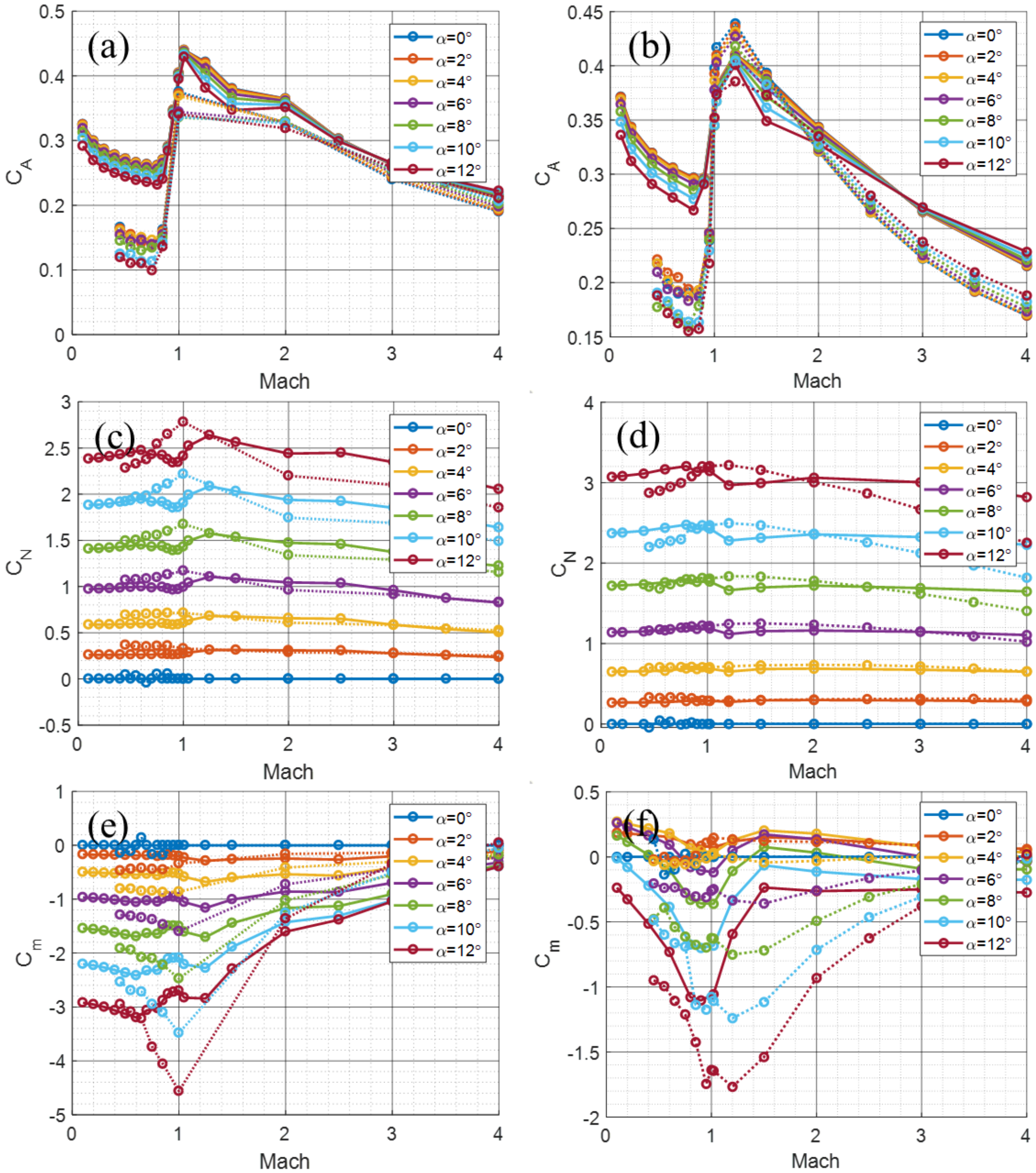

Fig. 5 Axial force (a-b), normal force (c-d), and pitching moment (e-f) coefficient across angle of attack and Mach number for both subsonic (a, c, e) and supersonic (b, d, f) optimal designs for Body-Fin configuration computed from Missile DATCOM (solid) and Cart3D (dashed)

Both Missile DATCOM and Cart3D data sources were combined in order to improve the overall accuracy of aerodynamic coefficients used in flight trajectory simulation. The static aerodynamic coefficients were compiled such that only the axial force coefficient used was computed by DATCOM, whereas all other static forces and moments were computed by Cart3D (e.g., C_N and C_m). For 6-DOF flight trajectory simulations, the dynamic derivatives computed from DATCOM were utilized. This methodology ensured a more accurate representation of the flight vehicle across Mach and angle of attack. The updated lift-to-drag ratios combining Cart3D and DATCOM for both optimal subsonic and supersonic designs are presented in Fig. 6a and b, respectively.

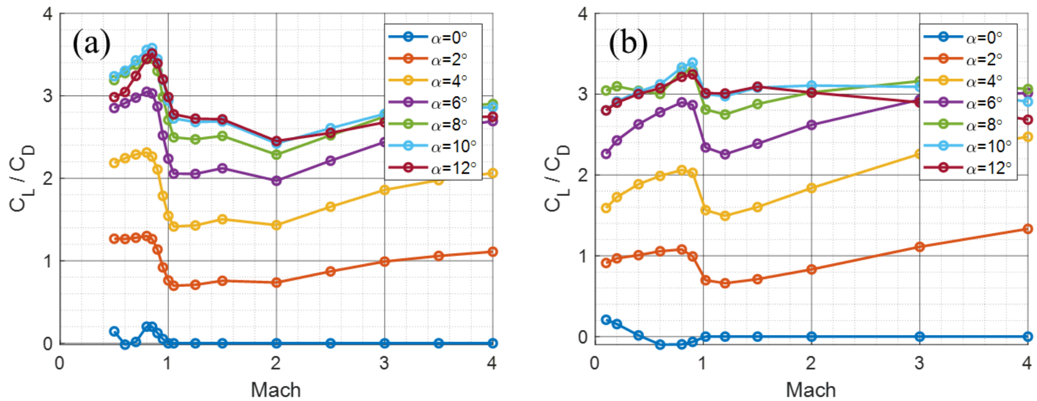

Fig. 6 Updated lift-to-drag ratios of both optimal a) subsonic and b) supersonic designs for Body-Fin configuration of 4-inch diameter, length-to-diameter of 1 0, and an ogive length of 30% of the overall length

4. Conclusion

A PSO method incorporating a semi-empirical aerodynamic prediction code (i.e., Missile DATCOM) was utilized to optimize the shape, size, and position of control surfaces for a given baseline body projectile. The optimization routine converged to designs that produced the maximum lift-to-drag at a body trim angle for each configuration. The selected designs were then further analyzed through the use of higher fidelity flow solvers in order to validate and to mature the aerodynamic model for each configuration. Further assessments of the optimal designs using higher fidelity flow solvers show that Missile DATCOM predicts the static aerodynamic coefficients reasonably well, suggesting that the routine is an efficient tool in the initial aerodynamic vehicle design process. Missile DATCOM was able to predict the normal force coefficient for high aspect ratio finned projectiles accurately at low angles of attack; however, it was not able to predict the pitching moment coefficient (and therefore center of pressure location) well. The aerodynamic data sources were compiled in a formal manner to improve the accuracy of the aerodynamic database used in flight trajectory simulations.

5. References

1. Foster NF, Dulikravich GS. Three-dimensional aerodynamic shape optimization using genetic and gradient search algorithms. Journal of Spacecraft and Rockets. 1997;34(1):36–42.

2. Tanrikulu Ö, Erca V. Optimal external configuration design of unguided missiles. Journal of Spacecraft and Rockets. 1998;35(3):312–316.

3. Lesieutre DJ, Dillenius MFE, Lesieutre TO. Multidisciplinary design optimization of missile configurations and fin planforms for improved performance. Proceedings of the 7th AIAA/USAF/NASA/ISSMO Symposium on Multidisciplinary Analysis and Optimization; 1998; St. Louis, MO. AIAA Paper 1998–4890.

4. Anderson MB, Burkhalter JE, Jenkins RM. Missile aerodynamic shape optimization using genetic algorithms. Journal of Spacecraft and Rockets. 2000;37(5)663–669.

5. Yang YR, Jung SK,Cho TH, Myong RS. Aerodynamic shape optimization system of a canard-controlled missile using trajectory-dependent aerodynamic coefficients. Journal of Spacecraft and Rockets. 2012;49(2):243–249.

6. Fowler L, Rogers J. Airframe performance optimization of guided projectiles using design of experiments. Journal of Spacecraft and Rockets. 2015;52(6):1603–1613.

7. Kennedy J, Eberhart, R. Particle swarm optimization. Proceedings of the IEEE International Conference on Neural Networks. 1995; Perth, Western Australia.

8. Eberhart R, Kennedy J. A new optimizer using particle swarm theory. Proceedings of the 6th International Symposium on Micro Machine and Human Science; 1995; Nagoya, Japan.

9. Venter G, Sobieszczanski-Sobieski J. Particle swarm optimization. Proceedings of the 43rd AIAA/ASME/ASCE/AHS/ASC Structures, Structural Dynamics, and Materials Conference; 2002; Denver, CO. AIAA Paper 2002–1235.

10. Shi Y, Eberhart R. A modified particle swarm optimizer. Proceedings of the IEEE International Conference on Evolutionary Computation; 1998; Anchorage, AK. p. 69–73.

11. Nickabadi A, Ebadzadeh M, Safabakhsh R. A novel particle swarm optimization algorithm with adaptive inertia weight. Applied Soft Computing. 2011;11(4):3658–3670.

12. Qin Z, Yu F, Shi Z,Wang, Y. Adaptive inertia weight particle swarm optimization. Proceedings of the Artificial Intelligence and Soft Computing – ICAISC 2006 8th International Conference; 2006; Zakopane, Poland. p. 450–459.

13. Reuther J, Jameson A. Aerodynamic shape optimization of wing and wing–body configurations using control theory. Proceedings of the AIAA 33rd Aerospace Sciences Meeting; 1995; Reno, NV. AIAA Paper 95–0123.

14. Leoviriyakit K, Jameson A. Aerodynamic shape optimization of qings including planform variations. Proceedings of the AIAA 41st Aerospace Sciences Meeting and Exhibit; 2003; Reno, NV. AIAA Paper 2003–0210.

15. Rosema C, Doyle J, Blake W. Missile DATCOM user's manual – 2014 Revision. Flight Dynamics Directorate, Wright Patterson Air Force Base (OH): Air Force Research Laboratory (US); 2014 Dec. Report No.: AFRL-RQ-WP-TR-2014-0281.

16. Aftosmis MJ, Berger MJ, Adomavicius G. A parallel multilevel method for adaptively refined Cartesian grids with embedded boundaries. 38th Aerospace Sciences Meeting and Exhibit; 2000; Reno, NV. AIAA Paper 2000–0808.

17. Strohm LS, Fresconi FE, Vasile JD. Long range precision fires: range extension study. Aberdeen Proving Ground (MD): CCDC Army Research Laboratory; 2019 Sep. Report No.: ARL-TR-8814.

18. Tian DP. A review of convergence analysis of particle swarm optimization. International Journal of Grid and Distributed Computing. 2013;6(6):117–128.

19. Doyle JB, Rosema CC. Vortex modeling improvements within missile DATCOM 2014. Redstone Arsenal (AL): Army Aviation and Missile Research, Development, and Engineering Center (US); 2016 May. Report No.: RDMR-SS-15-29.

20. Rosema CC, Doyle JB. Fin-shed vortex modeling within missile DATCOM. Proceedings of the 49th AIAA Aerospace Sciences Meeting including the New Horizons Forum and Aerospace Exposition; 2011 Jan; Orlando, FL. AIAA 2011–1240.

21. MATLAB 9.0. Natick (MA): The MathWorks, Inc [accessed 2020 Apr 8]. https://www.mathworks.com/products/matlab.html.

Nomenclature

x_{k+1}^{i}	updated position of particle *i* at iteration *k+1*
x_{k}^{i}	current position of particle *i* at iteration *k*
v_{k+1}^{i}	updated velocity of particle *i* at iteration *k + 1*
r_1, r_2	random numbers in the interval [0 1]
p_{k}^{i}	best position found by particle *i* so far in the optimization algorithm
p_{k}^{g}	current swarm's best particle position at iteration *k*
v_{k}^{i}	current velocity of particle *i* at iteration *k*
w_{k}^{i}	inertia parameter of particle *i* at iteration *k*
c_1	cognitive parameter
c_2	social parameter
α_{PSO}	positive constant in the interval [0 1]
ISA_{k}^{i}	Individual Search Ability parameter of particle *i* at iteration *k*
ϵ	positive constant close to zero, (i.e. $1 \cdot 10^{-6}$)
x_{0}^{i}	initial position of particle *i*
x_{min}	minimum design point in design space for given configuration
x_{max}	maximum design point in design space for given configuration
v_{0}^{i}	initial velocity of particle *i*
ϵ_{tol}	convergence criterion tolerance
$\bar{f}$	current mean fitness of the swarm (i.e., $\frac{\sum_{i=1}^{n} f(p_k^i)}{n}$)
n	number of particles in the swarm
M_∞	free stream Mach number
d	projectile diameter
l/d	length to diameter ratio
l_o	ogive length as percent of overall length of projectile

L/D	lift-to-drag ratio
D	drag coefficient
w_1	weight value for lift-to-drag objective
w_2	weight value for drag objective
w_3	weight value for static margin objective
SM	static margin
α	angle of attack
C_A	axial force coefficient
C_N	normal force coefficient
C_m	pitching moment coefficient
C_L	lift force coefficient
C_D	drag force coefficient

List of Symbols, Abbreviations, and Acronyms

CCDC-AvMC	US Army Combat Capabilities Development Command Aviation and Missile Center
CFD	computational fluid dynamics
DOD	US Department of Defense
DOF	degrees of freedom
DRSC	DOD Supercomputing Resource Center
NASA	National Aeronautics and Space Administration
OAL	overall length of the flight vehicle
PSO	Particle Swarm Optimization
SEAP	semi-empirical aerodynamic prediction

1	DEFENSE TECHNICAL
(PDF)	INFORMATION CTR
	DTIC OCA
1	CCDC ARL
(PDF)	FCDD RLD CL
	TECH LIB
2	CCDC AVMC
(PDF)	FCDD AMS MMA
	J DOYLE
	C ROSEMA
12	CCDC ARL
(PDF)	FCDD RLW A
	F FRESCONI
	FCDD RLW L
	W OBERLE
	FCDD RLW LE
	J VASILE
	J BRYSON
	J DESPIRITO
	L STROHM
	J PAUL
	V BHAGWANDIN
	L FAIRFAX
	B GRUENWALD
	I CELMINS
	FCDD RLW LF
	B TOPPER